

Group 2 innate lymphoid cells boost CD8⁺ T-cell activation in anti-tumor immune responses

Jing Wen^{a,b*}, Shipeng Cheng^{a*}, Ran Wang^{c*}, Yuying Huang^{a*}, Long Xu^{d*}, Liyan Ma^a, Zhiyang Ling^a, Jinfu Xu^{e#}, Deping Zhao^{d#}, Yaguang Zhang^{a,#}, and Bing Sun^{a#}

^aState Key Laboratory of Cell Biology, CAS Center for Excellence in Molecular Cell Science, Shanghai Institute of Biochemistry and Cell Biology, Chinese Academy of Sciences, University of Chinese Academy of Sciences, Shanghai, China; ^bSchool of Life Science and Technology, ShanghaiTech University, Shanghai, China; ^cSchool of Life Science, University of Science and Technology of China, Hefei, China; ^dDepartment of Thoracic Surgery, Shanghai Pulmonary Hospital, Tongji University School of Medicine, Shanghai, China; ^eDepartment of Respiratory and Critical Care Medicine, Shanghai Pulmonary Hospital, Institute of Respiratory Medicine, School of Medicine, Tongji University, Shanghai, China; ^fMed-X institute, Center for Immunological and Metabolic Diseases, the First Affiliated Hospital of Xi'an JiaoTong University, Xi'an JiaoTong University, Xi'an, Shaanxi, China

ABSTRACT

Group 2 innate lymphoid cells (ILC2s) are essential for orchestrating type 2 immune responses during allergic airway inflammation and infection. ILC2s have been reported to play a regulatory role in tumors; however, this conclusion is controversial. In this study, we showed that IL-33-activated ILC2s could boost CD8⁺ T-cell function through direct antigen cross-presentation. After activation by IL-33, ILC2s showed an enhanced potential to process antigens and prime CD8⁺ T cell activation. Activated ILC2s could phagocytose exogenous antigens *in vivo* and *in vitro*, promoting antigen-specific CD8⁺ T cell function to enhance antitumor immune responses. Administration of OVA-loaded ILC2s induces robust antitumor effects on the OVA-expressing tumor model. These findings suggested that the administration of tumor antigen-loaded ILC2s might serve as a potential strategy for cancer treatment.

ARTICLE HISTORY

Received 31 March 2023
Revised 11 July 2023
Accepted 27 July 2023

KEYWORDS

anti-tumor response; antigen presentation; CD8 T cell; ILC2

Introduction

Innate lymphoid cells (ILCs) are tissue-resident lymphocytes that sense diverse microenvironmental stress conditions and induce immune responses. Type 2 innate lymphoid cells (ILC2s) are a subgroup of ILCs that mainly express the transcription factors GATA3 and ROR α , and are involved in type 2 immune responses by secreting the cytokines IL-5 and IL-13.^{1–3} ILC2s are innate immune cells that closely mirror T-helper type 2 (Th2) cells.⁴ Both have been extensively studied in parasitic helminth infections and allergic diseases.⁵

Many studies have demonstrated that ILC2s are present in various tumors, including hematological malignancies, prostate cancer, bladder cancer, colorectal cancer, breast cancer, melanoma, and lung cancer.^{6,7} The role of ILC2s in tumors, particularly in tumor growth, has been reported to be a double-edged sword. With regard to their tumor-promoting effect, ILC2s can secrete type 2 cytokine IL-13 and recruit immunosuppressive myeloid-derived suppressor cells (MDSCs) to inhibit antitumor immune responses in some tumors, such as acute myeloid leukemia, prostate cancer, and bladder cancer.^{8–10} In contrast, to support antitumor immunity, ILC2s secrete cytokine granulocyte-macrophage colony-stimulating factor (GM-CSF) to recruit and activate eosinophils to enhance antitumor

responses¹¹. ILC2s also express PD-1 and anti-PD1 antibody therapy can increase CCL5 secretion in ILC2s, recruit dendritic cells (DCs), and activate T cells to enhance anti-tumor immune responses¹². PD-1 blockade on ILC2s can also promote TNF- α secretion to inhibit the progression of metastatic melanoma¹³. In addition, IL-9-secreting ILC2s activate CD8⁺ T cells to inhibit tumor growth¹⁴. Although a series of reports on the functions of ILC2s suggests that ILC2s have a certain function in antitumor immunity, the actual regulatory role of ILC2s in adaptive immune responses remains unclear. Therefore, a mechanistic study that reveals the function of ILC2s in anti-tumor immunity will provide benefits and aid in the development of new cancer treatment strategies.

ILC2s have been shown to form an intricate interaction loop with the adaptive immune system¹⁵. ILC2s affect the adaptive immune system through both direct and indirect mechanisms. ILC2-derived cytokines such as IL-5 and IL-13 can regulate the differentiation of Th2 cells and limit the immunosuppressive function of regulatory T cells (Tregs)^{1,16,17}. ILC2s secrete IL-5 and IL-6 to regulate B cells and support antibody production^{18,19}. ILC2s indirectly activate and prime CD8⁺ T cells via CCL5-recruited DCs, enhancing antitumor immune responses¹². Conversely, ILC2s can participate in immune regulation via crosstalk with adaptive immune cells

CONTACT Bing Sun  bsun@sibs.ac.cn  State Key Laboratory of Cell Biology, CAS Center for Excellence in Molecular Cell Science, Shanghai Institute of Biochemistry and Cell Biology, Chinese Academy of Sciences, University of Chinese Academy of Sciences, Shanghai, China

*J.W. Y.Z. S.C. R.W. Y.H. and L.X. contributed equally to this study.

#co-corresponding authors.

 Supplemental data for this article can be accessed online at <https://doi.org/10.1080/2162402X.2023.2243112>

© 2023 The Author(s). Published with license by Taylor & Francis Group, LLC.

This is an Open Access article distributed under the terms of the Creative Commons Attribution-NonCommercial License (<http://creativecommons.org/licenses/by-nc/4.0/>), which permits unrestricted non-commercial use, distribution, and reproduction in any medium, provided the original work is properly cited. The terms on which this article has been published allow the posting of the Accepted Manuscript in a repository by the author(s) or with their consent.

through surface molecules such as OX40L and inducible costimulatory ligand (ICOS-L) in cell contact-dependent interactions^{20,21}. Recently, the function of ILC2s as antigen-presenting cells was revealed. By directly interacting with CD4⁺ T cells through MHCII, ILC2s promote Th2 polarization and cytokine production in CD4⁺ T cells⁵. In addition, ILC2s in the human skin can express CD1a, an endogenous lipid antigen-presenting molecule on antigen-presenting cells (APCs), to directly activate CD1a-reactive T cells and thus contribute to skin inflammation²². Thus far, research has predominantly focused on the role of ILC2s in the presentation of antigens to CD4⁺ T cells. However, whether ILC2s can present antigens to CD8⁺ T cells remains unknown.

Tumor-infiltrating CD8⁺ T cells are the central component of antitumor immune responses in cancer-specific immunity. CD8⁺ T cells must be activated by APCs presenting tumor-specific antigens on MHC-I at the beginning of protective immunity to acquire an adequate capacity to kill tumor cells²³. Generally, intratumoral APCs capture and process neoantigens derived from tumor cells and load them onto MHC-I complexes on the cell surface. APCs also provide costimulatory signaling to induce potent T-cell functions. During these interactions, naïve CD8⁺ T cells become tumor-specific CD8⁺ T cells that are capable of killing target tumor cells. Therefore, priming and activation of CD8⁺ T cells are critical for successful antitumor immunity.

We hypothesized that the administration of activated ILC2s capable of capturing tumor antigens would be an effective antitumor biotherapy. We isolated IL-33-activated ILC2s and assessed the expression of MHC-I and costimulatory molecules. Activated ILC2s displayed antigen phagocytosis to prime CD8⁺ T cell activation, which was antigen-dependent. The antigen-loaded ILC2s administered intravenously induced significant antitumor efficacy in antigen-specific murine models. Together, we conclude that IL-33-activated ILC2s can inhibit tumor growth through cross-presenting antigens to activate CD8⁺ T cells.

Results

ILC2s have antigen processing and presentation potential after activation

ILC2s can serve as APCs that mediate CD4⁺ T cell activation via MHC-II⁵. To investigate whether ILC2s have the molecular signature necessary to process and present antigens to CD8⁺ T cells, we analyzed the transcriptome of naïve and IL-33-activated lung ILC2s using RNA sequencing (RNA-seq). Activated ILC2s were obtained from IL-33 or papain-induced acute pulmonary inflammation model (Figure S1a,b). Naïve ILC2s from unchallenged mice were purified from 6 to 8 weeks C57BL/6 females. Murine lung ILC2s were stained according to the surface marker phenotype FVS⁻CD45⁺Lin⁻CD90.2⁺ST2⁺ (Figure S1c). ILC2 populations showed purity higher than 99% (Figure S1d). ILC2 populations were also identified using real-time quantitative polymerase chain reaction (qRT-PCR) (Figure S1e,f). Gene set enrichment analysis (GSEA) showed the enrichment of the MHC protein complex (Figure 1a). A heatmap of the RNA-seq results demonstrated that MHC-I-associated molecules, including light

chain β 2 microglobulin (B2M) and heavy chain highly polymorphic genes (H-2K, H-2D, and H-2L),²⁴ as well as the costimulatory molecules²⁵, were upregulated in activated ILC2s (Figure 1b). Activated ILC2s showed similar gene upregulation profiles to DCs after LPS stimulation (Figure S1g), which were obtained from the published profiles in GSE184976. And the enrichment and upregulation of processing-associated genes in activated ILC2s were consistent with that of MHC-I-associated genes (Figure 1c,d). qRT-PCR data verified that IL-33-activated ILC2s exhibited higher levels of MHC-I-associated molecules than naïve ILC2s at the transcriptional level (Figure 1e,f). We also found that IL-33 stimulation increased the expression of MHC-I genes in a time-dependent manner (Figure 1g). The upregulation of CD80 and CD86 in activated ILC2s was confirmed at the transcriptional level (Figure 1h,j). A certain percentage of ILC2s also expressed the costimulatory molecules, CD80 and CD86, at the protein level (Figure 1i,k). These results suggested that IL-33 activated ILC2s had the potential to process and present antigen via the MHC-I pathway. We used activated ILC2s for subsequent experiments.

ILC2s phagocytose antigens *in vitro* and *in vivo*

FITC-dextran was used to evaluate the endocytic activity of the murine ILC2s.²⁶ ILC2s were obtained from IL-33-induced murine lung tissue. ILC2s were incubated with 0.2 mg/ml FITC-dextran for 40 min and then analyzed by flow cytometry to assess phagocytosis (Figure 2a). ILC2s incubated without FITC-dextran or with FITC-dextran for 40 min at 4°C were set as controls. The increased FITC-dextran expression of ILC2s suggested that ILC2s had the capacity for phagocytosis. Next, we tested whether ILC2s captured antigenic proteins derived from tumor cells. The B16F10-SOVA cell line is a variant of B16F10 melanoma cells that simultaneously express ovalbumin (OVA) as a tumor antigen and the fluorescent protein mCherry as a marker to track antigen phagocytosis. ILC2s were cocultured with B16F10-SOVA, and mCherry expression on ILC2s was analyzed by flow cytometry. ILC2s showed more mCherry positive percentage as time went on (Figure 2b). We intravenously injected B16F10-SOVA tumor cells to establish a lung metastatic tumor model (Figure 2c). Fourteen days after implantation, we profiled the CD90.2⁺ immune cells in the lung by flow cytometry (Figure 2d). mCherry fluorescence in immune cells, derived from the tumor, was assessed. Approximately 6% of ILC2s (CD45⁺Lin⁻CD90.2⁺ST2⁺) were mCherry⁺, which was higher than other cell subsets (Figure 2e). mCherry loading revealed that ILC2s engulfed tumor-derived antigens *in vivo*. We also confirmed that the proportion of mCherry⁺ ILC2s increased as the tumor grew (Figure 2f), increasing from <1% of ILC2s at the early stage to nearly 20% of ILC2s at the late stage (Figure 2g). Besides, ILC2s isolated from B16F10-OVA metastases induced OT-I CD8⁺ T cells expressing CD69 (Figure 2h). Taken together, ILC2s were able to phagocytose antigens *in vitro* and *in vivo*.

ILC2s form cell clusters with CD8⁺ T cells in an antigen-dependent manner

To elucidate the interaction between ILC2s and CD8⁺ T cells, we developed a real-time cell imaging co-culture system to

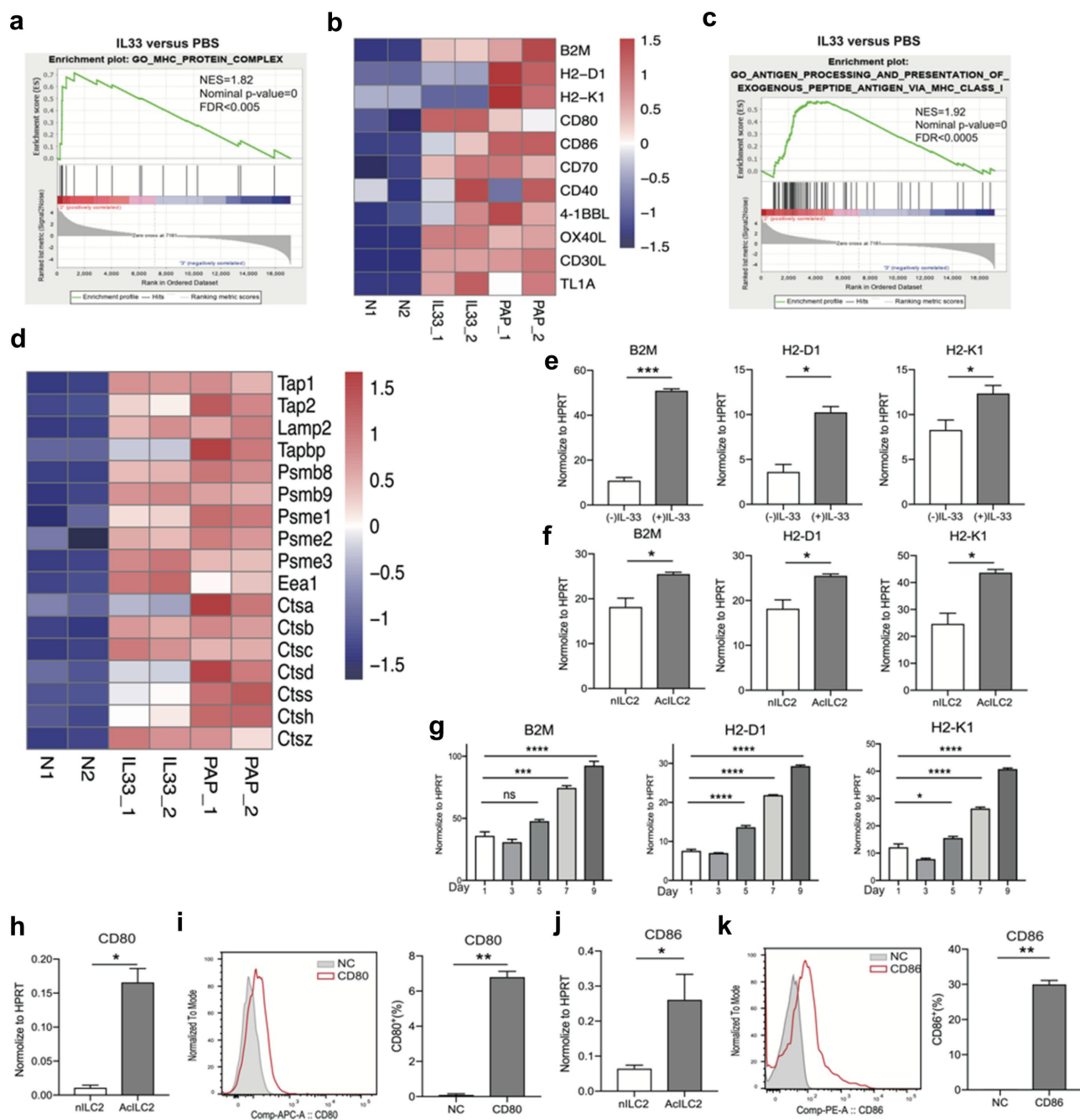


Figure 1. IL-33-activated ILC2s upregulated MHC-I molecules and molecules related to antigen processing and presentation. (a) GSEA enrichment analysis identifying the MHC-I protein complex in activated ILC2s. NES, normalized enrichment score; FDR, false discovery rate. (b) Heatmap of the \log_2 -transformed expression of selected MHC class I-associated molecules and costimulatory molecules from RNA-sequencing data across populations. (c) GSEA enrichment analysis showing enrichment of the antigen processing and presentation of peptide antigen via MHC class I pathway. (d) Heatmap of the \log_2 -transformed expression of selected cathepsin proteins and antigen processing-related genes. (e) RT-PCR analysis of the expression of the heavy and light chains of MHC-I: B2M, H2-D1, and H2-K1. (f) RT-PCR analysis of the expression of the heavy and light chains of MHC-I in ILC2s stimulated with IL-33 for 3 days *in vitro*. (g) The levels of the heavy and light chains of MHC-I in IL-33-stimulated ILC2s were analyzed on different days by RT-PCR. (h) The level of CD80 in ILC2s was analyzed by RT-PCR. (i) Representative flow cytometric histogram overlays and quantitative analysis of CD80 expression on ILC2s from IL-33-treated mice. (j) The level of CD86 in ILC2s was analyzed by RT-PCR. (k) Representative flow cytometric histogram overlays and quantitative analysis of CD86 expression on ILC2s from IL-33-treated mice. For RNA seq and cytometric data, $n = 2$ mice per group; for RT-PCR, $n = 2$ replicates in each experiment. Data are shown as the means \pm SEMs. The p value was determined by one-way ANOVA. *, $p < 0.05$; **, $p < 0.01$; ***, $p < 0.001$; ns, not significant.

monitor CD8⁺ T cell – ILC2 interactions. IL-33-activated ILC2s from Red5 (IL5^{tdtomato-cre}) mice were cocultured with OT-I CD8⁺ T cells with or without OVA protein. A series of representative images of T-cell-ILC2 interactions are shown in Figure 3a, and movies are shown in Movie S1. There were only

random collisions in the CD8 alone group, the group treated with ILC2s alone, and the group treated with OVA protein alone. The T-cell-ILC2 interaction could be detected in the presence of exogenous soluble OVA and ILC2s. The numbers and relative area ratio of CD8⁺ T-ILC2 cell clusters per field

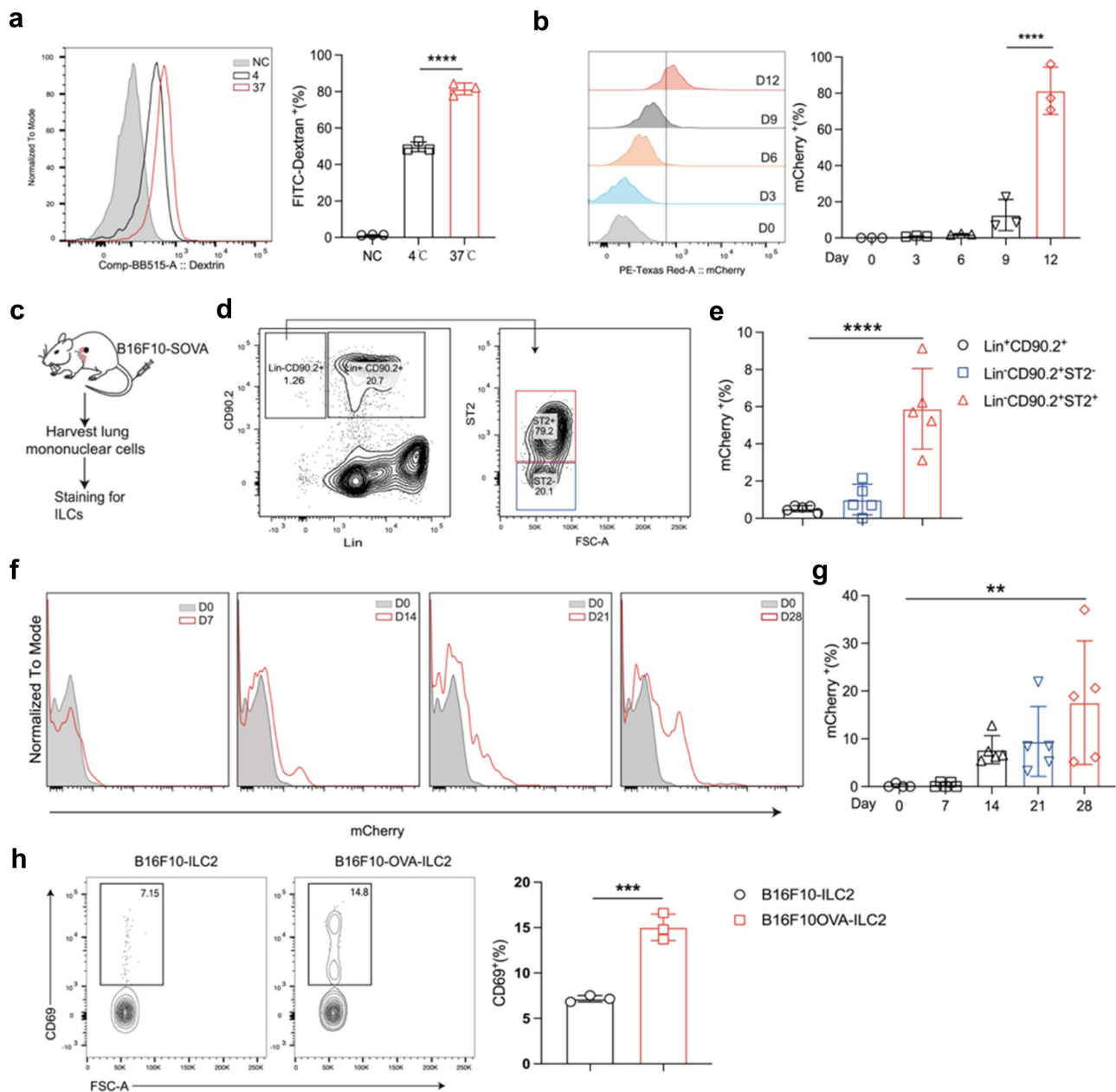


Figure 2. ILC2s phagocytosed antigens *in vitro* and *in vivo*. (a) Flow cytometric histogram overlays and quantitative analysis depicting *in vitro* uptake of FITC-dextran by ILC2s ($n = 3$ independent wells). (b) Analysis of tumor-derived mCherry fluorescence in ILC2s cocultured with B16F10-SOVA tumor cells ($n = 3$ independent wells). (c) Schematic showing the strategy for the lung metastasis model. (d) Representative flow cytometry plot and gating of tumor-infiltrating immune cells. (e) Frequency of mCherry⁺ immune cells across tumors ($n = 5$ mice per group). (f) Representative flow cytometric histograms of tumor-derived mCherry fluorescence within tumor-infiltrating ILC2s from day 7 through day 28. (g) Frequency of mCherry⁺ ILC2s in the tumor over the course of tumor progression ($n = 5$ mice per group). (h) Flow cytometry plot and frequency of CD69⁺ CD8 were analyzed by flow cytometry ($n = 3$ independent wells). Data are shown as the means \pm SEMs. The p value was determined by one-way ANOVA. *, $p < 0.05$; **, $p < 0.01$; ***, $p < 0.001$; ns, not significant.

increased over time (Figure 3b,c). Therefore, this imaging data showed that OT-CD8⁺ T cells formed cell clusters around ILC2s loaded with OVA antigen *in vitro*.

ILC2s promote CD8⁺ T-cell proliferation and cytokine secretion upon antigen stimulation

Next, we investigated the antigen-presenting and antigen-processing functions of ILC2s to CD8⁺ T cells. Activated ILC2s were incubated with CellTrace Violet (CTV)-labeled OVA-specific transgenic OT-I CD8⁺ T cells for 3 days with or without an exogenous soluble SIINFEKL peptide (OVA₂₅₇₋₂₆₄). The

percentage of proliferating T increased significantly after the addition of ILC2s (Figure 4a). In addition, we investigated whether ILC2s could prime OT-I CD8⁺ T-cell proliferation by processing and presenting soluble OVA protein. Nearly 60% of OT-I CD8⁺ T cells proliferated when both OVA protein and ILC2s were present (Figure 4b). In contrast, CD8⁺ T cells failed to proliferate when they were cultured alone, with only the OVA protein, or co-cultured with ILC2s without the OVA protein (Figure 4b). ILC2s generally act on other immune cells by secreting effector cytokines such as IL-9 and GM-CSF. We isolated OVA-loaded ILC2s and their supernatants, and co-cultured with CTV-labeled OT-I CD8⁺ T cells, respectively. Results showed that

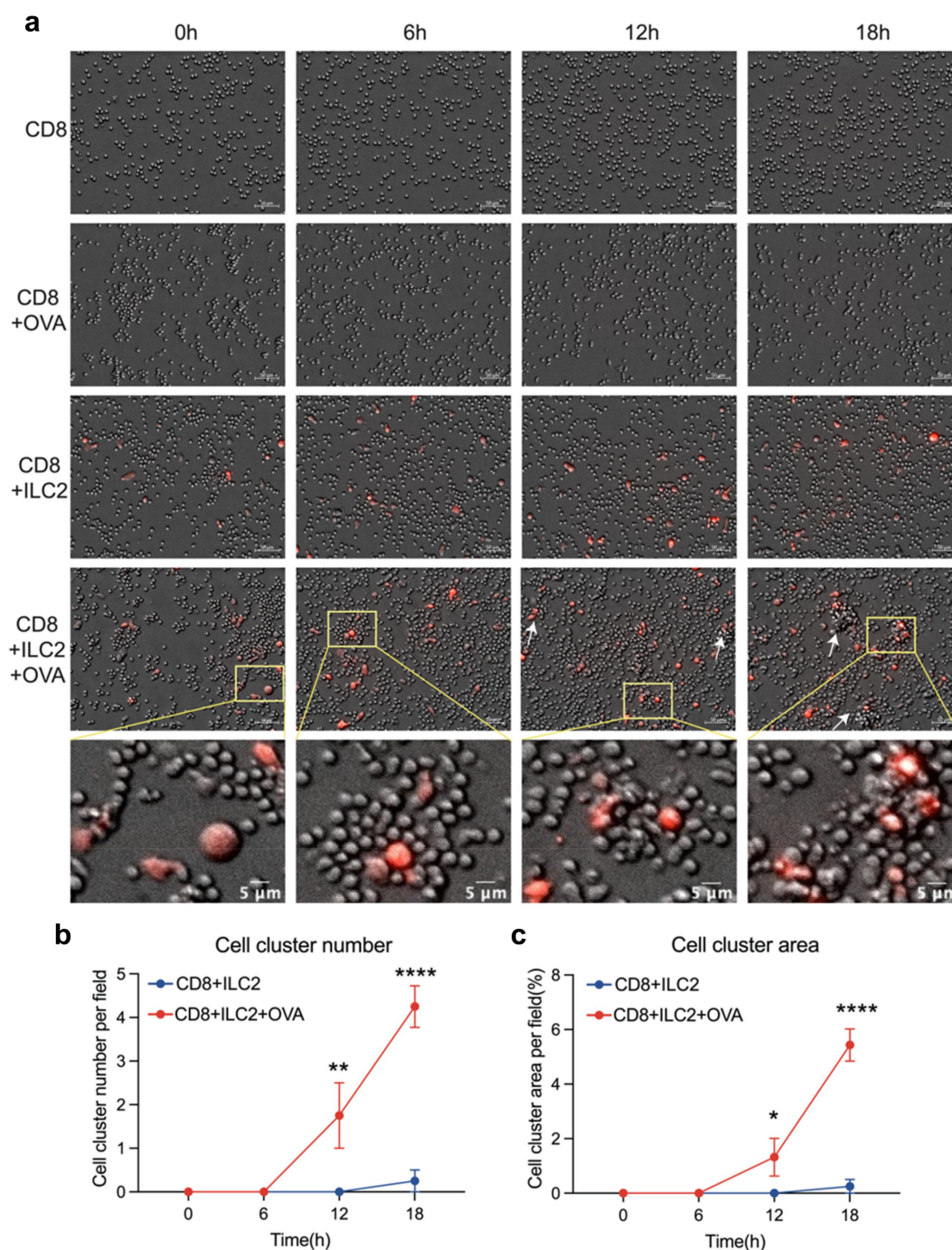


Figure 3. ILC2s formed cell clusters with CD8⁺ T cells in the presence of antigen. (a) the cells showing red fluorescence are ILC2s, whereas those with no fluorescence are CD8⁺ T cells. ILC2s (2×10^4) were cocultured with CD8⁺ T (6×10^5) cells for 20 hours. Live cell imaging of ILC2-CD8⁺ T-cell interactions at different time points revealed that the cells formed constant cell clusters during the coculture. Scale bar = 50 μ m or 5 μ m. (b) Statistical analysis of cell cluster number per field ($n = 4$ views per well). (c) Statistical analysis of cell cluster area percentage per field ($n = 4$ views per well). Data are shown as the means \pm SEMs. The p value was determined by two-way ANOVA. *, $p < 0.05$; **, $p < 0.01$; ***, $p < 0.001$; ns, not significant.

only OVA-loaded ILC2s stimulated T-cell proliferation; the supernatants failed to promote T-cell proliferation (Figure 4c). Next, we used myelin oligodendrocyte glycoprotein-MOG protein as a control antigen to test whether MOG-loaded ILC2s could promote OT-I CD8⁺ T cell proliferation. Only OVA-loaded ILC2s stimulated OT-I CD8⁺ T-cell proliferation; the MOG-loaded failed to promote OT-I CD8⁺ T-cell proliferation (Figure 4d). And ILC2s promoted cytokine IFN- γ , TNF- α and Granzyme B (GZMB) production of OT-I CD8⁺ T cells with OVA

stimulation (Figure 4e-g). These data suggested that ILC2s promoted CD8⁺ T cell proliferation and function with specific antigen stimulation.

Antigen-loaded ILC2s induce robust tumor killing

We examined whether OVA-loaded ILC2s enhance CD8⁺ T cell cytotoxicity against B16F10-OVA cells that express OVA

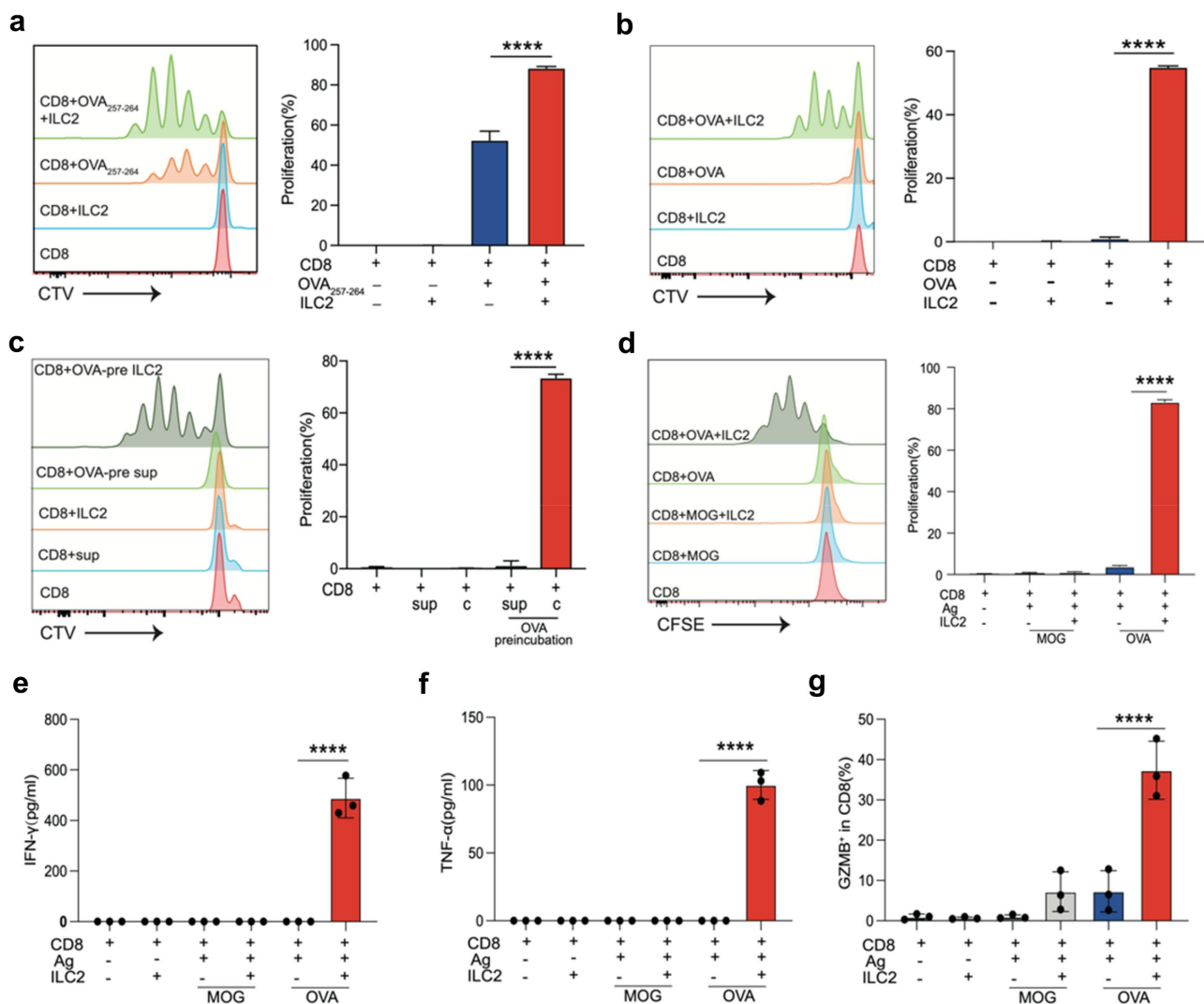


Figure 4. ILC2s promoted OT-I CD8⁺ T-cell proliferation and cytokine production with OVA-stimulation. (a) Analysis of CD8⁺ T-cell proliferation using CTV by flow cytometry as described in the Methods. CTV-labeled OT-I CD8⁺ T cells were cultured with ILC2s in the absence or presence of 10 μM OVA₂₅₇₋₂₆₄. CD8⁺ T-cell proliferation was measured by flow cytometry, as shown in the histograms. Column chart showing the percentages of proliferating OT-I CD8⁺ T cells ($n = 3$ independent wells). (b) CTV-labeled OT-I CD8⁺ T cells were cultured with ILC2s in the absence or presence of soluble OVA protein. CD8⁺ T-cell proliferation was measured by flow cytometry ($n = 3$ independent wells). (c) After pretreatment with or without the OVA protein, isolated ILC2s and supernatants were separately cultured with CD8⁺ T cells. CD8⁺ T-cell proliferation was measured by flow cytometry ($n = 3$ independent wells). (d) CFSE-labeled OT-I CD8⁺ T cells were cultured with ILC2s in the absence or presence of soluble OVA protein or MOG protein. CD8⁺ T-cell proliferation was measured by flow cytometry ($n = 3$ independent wells). (e–f) the IFN-γ and TNF-α protein levels in the supernatants were detected by ELISA ($n = 3$ independent wells). (g) the percentage of GZMB⁺ in CD8⁺ T cells were detected by flow cytometry ($n = 3$ independent wells). Data are shown as the means ± SEMs. The p value was determined by one-way ANOVA. *, $p < 0.05$; **, $p < 0.01$; ***, $p < 0.001$; ns, not significant.

antigens. Antigen-loaded ILC2s were cocultured with OT-I CD8⁺ T and B16F10-OVA cells (Figure 5a). We chose MOG as another antigen control. The release of LDH in the supernatant of OVA-loaded ILC2 significantly increased after 24 h of coculture compared with CD8⁺ T cells alone or MOG-loaded ILC2-T cell coculture systems (Figure 5b). Moreover, OVA-loaded ILC2s drove CD8⁺ T cells to exhibit robust tumor-killing function within 3 days, while control MOG-loaded ILC2s did not show such phenotype (Figure 5c). These indicated that antigen-uploaded ILC2s boost CD8⁺ T cells tumor killing ability *in vitro*. To test whether OVA-loaded ILC2s could enhance antitumor responses *in vivo*, we generated a subcutaneous mouse model using co-transplantation of ILC2s and B16F10-OVA tumor cells (Figure 5d). The co-transplantation of ILC2s indeed increased the proportion of ILC2s in tumor tissues (Figure S2a). OVA-

loaded ILC2s delayed significantly tumor growth *in vivo* (Figure 5e), and the tumor size in OVA-loaded ILC2s were smaller than that in control group at endpoint (Figure 5f). In addition, we observed that the percentage of CD8⁺ T cells in the ILC2-mixed group was significantly higher than that in the control group (Figure 5g). And Treg infiltration decreased (Figure 5h) and the CD8⁺ T cell/Treg ratio increased (Figure 5i). Thus, these results demonstrated that OVA-loaded ILC2s decreased tumor development.

Antigen-loaded ILC2s inhibit B16F10-OVA lung metastasis

We next determined whether ILC2s loaded with OVA would inhibit B16F10 lung metastasis. OVA-loaded ILC2s were injected

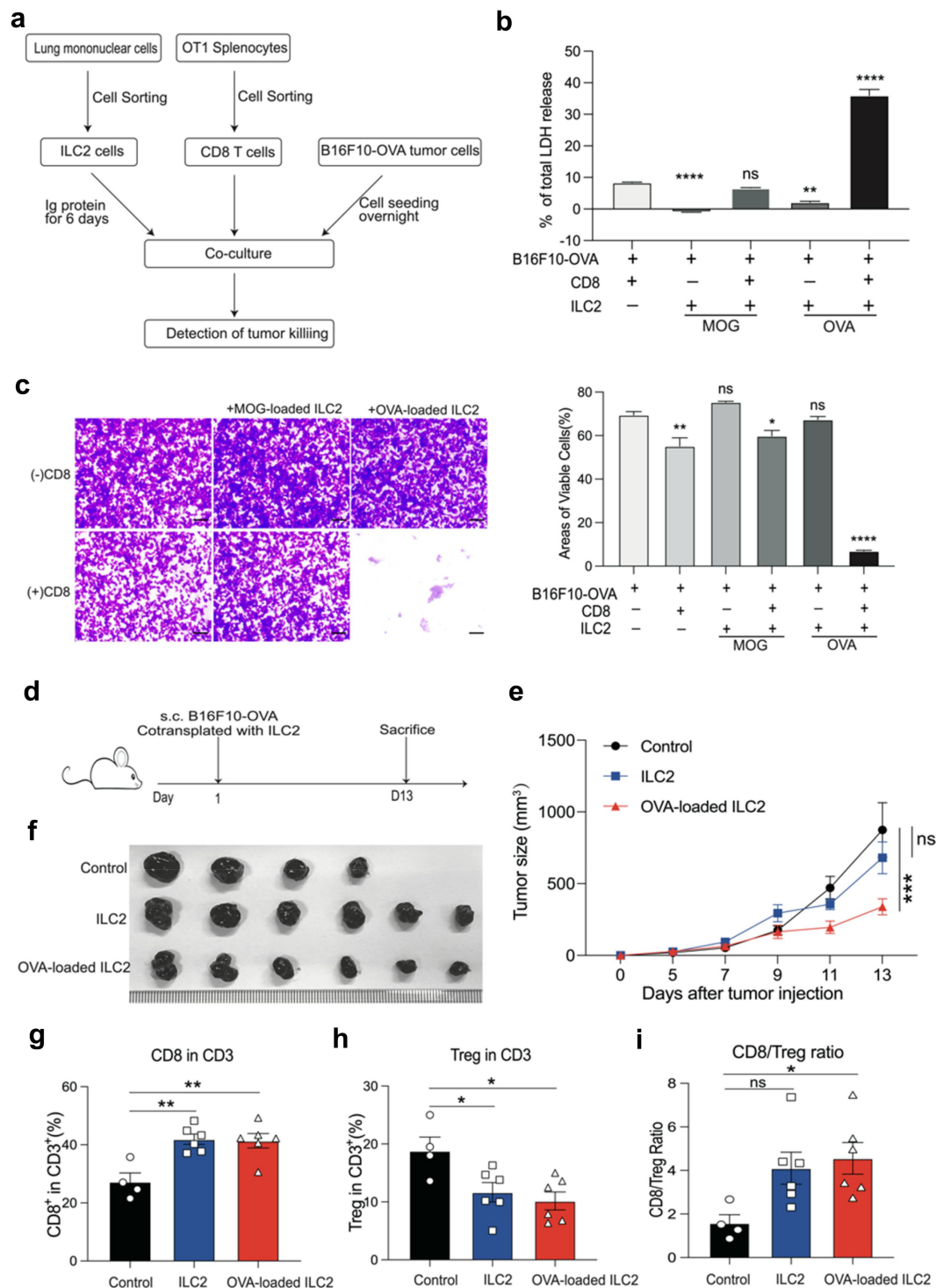


Figure 5. OVA-loaded ILC2s increased CD8⁺ T cells cytotoxicity and delayed antigen-specific tumor growth. (a) Schematic diagram of the experimental design. Activated ILC2s were loaded with OVA protein or MOG protein. The ratio of OT-I CD8⁺ T cells to tumor cells was 10:1. (b) Representative data for LDH release from B16F10-OVA cells after treatment with OT-I CD8⁺ T cells induced by ILC2s ($n = 3$ independent wells). (c) Representative images of B16F10-OVA cells stained with crystal violet after co-culture with OT-I CD8⁺ T cells. Statistical analysis of the areas of living cells at the bottom of the plate was performed ($n = 3$ views per well). Data are shown as the mean \pm SEMs. The p value was determined using one-way ANOVA. *, $p < 0.05$; **, $p < 0.01$; ***, $p < 0.001$; ns, not significant. (d) B16F10-OVA (2×10^5 mixed with OVA loaded or not ILC2s (2×10^5) were inoculated subcutaneously until the maximum tumor reached ~ 1000 mm³. (e–f) Tumor growth curve and volume in different treatment groups ($n = 4$ –6 mice per group). Data are shown as the mean \pm SEMs. The p value was determined using a two-way ANOVA. *, $p < 0.05$; **, $p < 0.01$; ***, $p < 0.001$; ns, not significant. (g–i) the percentages of CD8⁺ T cells and Treg cells and cell ratio in the tumors of ILC2- and OVA-loaded ILC2-treated mice and control mice ($n = 4$ –6 mice per group). Data are shown as the mean \pm SEMs. The p value was determined by one-way ANOVA. *, $p < 0.05$; **, $p < 0.01$; ***, $p < 0.001$; ns, not significant.

intravenously at 1×10^5 /injection every other day until endpoint (Figure 6a). We observed that the proportion of ILC2s increased in ILC2 adoptive transfer group (Figure S2b). OVA-loaded ILC2s significantly inhibited the formation of lung metastases from

B16F10-OVA clones (Figure 6b–d). OVA-loaded ILC2s decreased lung weight at the endpoint (Figure 6e)²⁷. Consistent with the results in the subcutaneous co-transplanted tumor, OVA-loaded ILC2s increased CD8⁺ T cells percentage and decreased Treg

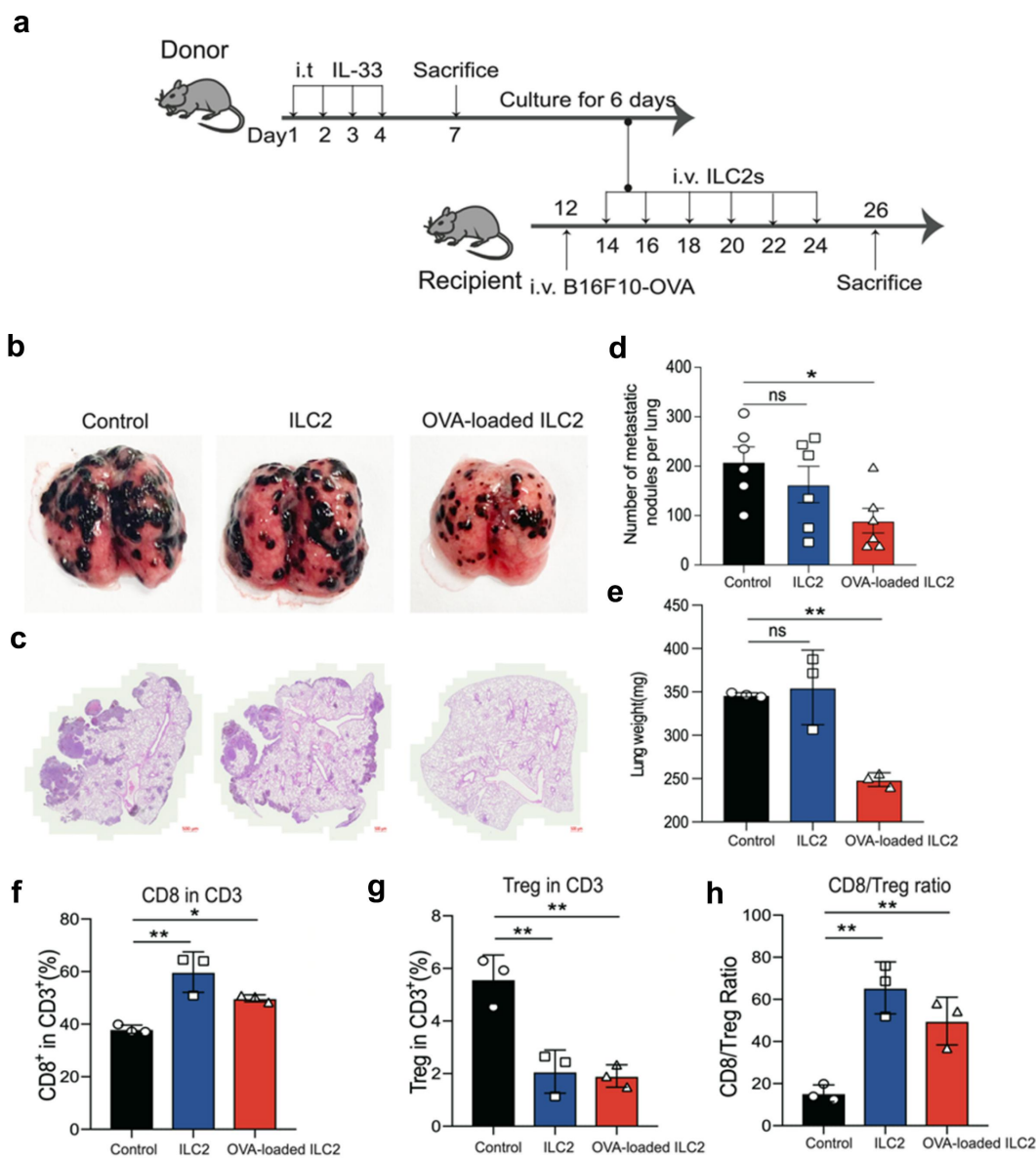


Figure 6. Adoptive transfer of OVA-loaded ILC2s inhibited B16F10-OVA lung metastasis. (a) Schematic diagram showing strategy for OVA-loaded ILC2s adoptive transfer treatment in lung metastasis model. (b) Representative pictures of lung tumor clones. (c) Representative photomicrographs of haematoxylin/eosin(HE)-stained lung sections. (d) the metastatic tumor nodules in lung in different treatment group ($n = 6$ mice per group). (e) the lung weight in different treatment group ($n = 3$ mice per group). (f–h) the percentages of CD8⁺ T cells and Treg cells and cell ratio in the tumors of ILC2- and OVA-loaded ILC2-treated mice and control mice ($n = 3$ mice per group). Data are shown as the means \pm SEMs. The p value was determined by one-way ANOVA. *, $p < 0.05$; **, $p < 0.01$; ***, $p < 0.001$; ns, not significant.

percentage, leading to elevated CD8/Treg ratio in the tumor microenvironment (Figure 6f–h). Meanwhile, we analyzed other immune cell subsets in B16F10-OVA metastatic lung tissue. The proportion of DC, NK, and conventional T cells in CD45⁺ cells showed no obvious variation (Figure S2c–e). In bronchoalveolar lavage fluid (BALF), there were no significant changes in the percentage of eosinophil, macrophage, and neutrophils in CD45⁺ cells after OVA-loaded ILC2s treatment (Figure S2f–h). Taken together, these results indicated that ILC2s loaded with OVA significantly inhibited B16F10-OVA metastasis.

Discussion

The function of ILC2s in tumors remains elusive, with these cells showing either antitumor or tumor effects, depending on

the cancer type. Although the fact that ILC2s present antigen to CD4⁺ T cells in inflammatory diseases has been described⁵, whether ILC2s cross-present tumor-derived antigens to CD8⁺ T cells have not yet been explored. In this study, we demonstrate that ILC2s phagocytose and process antigens to prime CD8⁺ T cell activation and ILC2s loaded with antigen can induce robust efficacy in inhibiting tumor growth. Activation and function of T cells are initiated by cognate antigens presented by APCs. ILC2s show upregulated antigen processing and presenting gene profiles after IL-33 stimulation, which is similar to DCs after LPS stimulation. A previous study demonstrated that MHC-II and costimulatory CD80 and CD86 expressed on ILC2s contributed to CD4⁺ T cell activation and then promoted type 2 immune response, which indicated the functions of ILC2s as APCs⁵. We showed that ILC2s

upregulated MHC class I molecules, costimulatory molecules, and gene profiles involved in antigen processing and presentation after IL-33 activation. The enrichment of costimulatory molecules in IL-33-activated ILC2s is consistent with the previous study that IL-33 promotes costimulatory protein OX40L expression on ILC2s to enhance CD8⁺ T cell-dependent antitumor effects²⁸.

We find that IL-33-activated ILC2s have antigen phagocytosis and then initiate CD8⁺ T cell activation and proliferation. ILC2s take up antigens from the surrounding environment and form cell clusters with CD8⁺ T cells in an antigen-dependent manner, which is supposed to be a fundamental factor for T cell activation. The OVA-loaded ILC2s induce OT-I CD8⁺ T cell proliferation and cytokine production. This is of particular importance because antigen-specific CD8⁺ T cells have critical roles in inhibiting tumors. The results of superior tumor suppression from coculture systems of OVA-loaded ILC2s with OT-I CD8⁺ T cell and B16F10 tumor cells indicate that antigen-specific ILC2-CD8 crosstalk contributes to enhancing antitumor effects. Previous studies have demonstrated that ILC2-derived cytokines, like IL-9 and TNF- α , are also helpful to antitumor immune responses^{13,14}. It is therefore evident that the role of ILC2s in anti-tumor immune response is driven by multiple mechanisms.

We demonstrate that OVA-loaded ILC2s have robust antitumor efficacy in both the subcutaneous co-transplantation model and lung metastasis tumor model. Previous studies have reported that DC and monocyte loaded with antigens can be used as a therapeutic cell-based treatment or cancer vaccine, which induce strong antigen-specific cytotoxic lymphocyte responses^{29,30}. Activated ILC2s can also be loaded with antigen protein, which is similar to that on DC or monocytes. Administration of antigen-loaded ILC2s increases the proportions of tumor-infiltrating CD8⁺ T cells to inhibit tumor growth. Preliminary data showed there was no change in the proportion of other immune cells in the tumor microenvironment, like DC and NK, after antigen-loaded ILC2s treatment. However, whether these immune cells are functionally involved in the change of tumor microenvironment is unclear.

Although our study demonstrates that IL-33-activated ILC2s have antitumor function by presenting exogenous antigen to CD8⁺ T cells, whether tumor infiltrating ILC2s have endogenous antigen presentation ability has not yet been explored. ILC2s and ILC3s can process and present antigens to CD4⁺ T cells through MHC-II and costimulatory molecules^{5,31,32}. However, the direct comparison of antigen-presenting ability between ILC2s and other classic APCs remains unclear. The previous study provides some hints that MHC-II expression on IL-33-elicited ILC2s is less than DC and B cell, which suggest that the antigen-presenting capacity of ILC2s might be lower than DC and B cells⁵. We assume that ILC2s-activated CD8⁺ T cells via antigen-presenting process have a place on antitumor immunity, especially in the ILC2 resident tissue, such as the lung. The potency of ILC2s delivering specific antigen signaling to CD8⁺ T deserves further deep exploration. Transportation of tumor antigen by migrating DCs is critical to prime antitumor immune responses³³. Whether ILC2s have a similar migration pattern to classic APCs during tumor development is also fascinating to explore.

IL-33 triggered ILC2s activation is accompanied by a series of molecular and cellular changes, including unexpected antigen processing and presenting associated genes and costimulatory molecules. Exploring whether there is a difference in antigen-presenting gene profile between ILC2s and DC might help deepen the understanding of the ILC2-CD8⁺ T cell axis in the tumor microenvironment.

In summary, this study provides a new understanding of the crosstalk between ILC2s and CD8⁺ T cells, which promotes antitumor immunity. IL-33-activated ILC2s loaded with antigen induce CD8⁺ T cell activation and robust antitumor responses in mice and have the possibility of potential clinical application. Additionally, ILC2s-based cell therapy provides the possibility of combining with other immunotherapies, such as checkpoint blockade or DC vaccines, to enhance therapeutic efficacy.

Methods

Mice

C57BL/6 mice were purchased from Shanghai Silaike Experimental Animal Co. Ltd. (Shanghai, China). Red5 mice (IL-5^{tdtomato-cre}) were obtained from the Chinese Academy of Sciences (Shanghai, China). All experimental animals used and analyzed were female, with an average age of 6–8 weeks. All animals were bred and housed in specific pathogen-free (SPF) facilities at the Center for Excellence in Molecular Cell Science at a constant temperature under a regular 12-hour light/12-hour dark cycle. All animal experimental protocols were approved by the Institutional Animal Care and Use Committee of the Center for Excellence in Molecular Cell Sciences.

Tumour cell lines

The B16F10-OVA cell line was kindly provided by Yong Cang (Shanghai Scholar University, Shanghai, China), and the B16F10-SOVA cell line was kindly provided by Chenqi Xu (Center for Excellence in Molecular Cell Sciences, CAS, Shanghai, China), respectively. The B16F10-SOVA cell line is a variant of the B16F10 cell line, which stably expresses the fluorescent protein mCherry and the specific antigen OVA. All tumor cells were cultured in complete DMEM containing 10% fetal bovine serum (FBS) and 1% penicillin/streptomycin (Gibco). All cells were cultured in a humidified incubator at 37°C with 5% carbon dioxide.

Tumour challenge and treatment

For lung metastasis mouse models, 2×10^5 B16F10-OVA or B16F10-SOVA cells were injected into each mouse via tail vein. Mice were intravenously (i.v.) injected with 1×10^5 ILC2s or OVA-loaded ILC2s every 2 days beginning on the second day after the tumor cell injection. Lungs of mice were removed after 14 days. The number of metastatic nodules on the lung surface and lung weight were counted. For co-transplantation experiments, 2×10^5 B16F10-OVA cells were co-transplanted with 2×10^5 ILC2s or OVA-loaded ILC2s. Tumor cells mixed with ILC2s at a 1:1 ratio were subcutaneously injected. Tumor

size was measured using a digital caliper and tumor volume was calculated as length \times width \times width. Transplanted tumors were harvested when the larger masses approximately reached $\sim 1000 \text{ mm}^3$.

Tissue processing

For lung mononuclear cell isolation, the experimental mice were euthanized by CO_2 asphyxiation and intracardially perfused with cold PBS to remove blood from the mouse lungs. The lungs were removed, cut into small pieces with scissors, and then incubated in dissociation buffer (RPMI-1640 medium containing 10% FBS, 1% penicillin/streptomycin, and 0.5 mg/ml collagenase type I) for 30 min at 37°C in a shaking incubator. After digestion, the tissue suspension was dissociated mechanically through a $70\text{-}\mu\text{m}$ filter and centrifuged at $350 \times g$ for 5 min. The supernatant was discarded and the pellet was resuspended in 40% Percoll (GE Healthcare). The cell suspension was then gently layered on top of 80% Percoll solution. Lung mononuclear cells were enriched by Percoll gradient centrifugation at $600 \times g$ for 20 min and isolated for further experiments and analysis. Splenocytes and lymph node cells were mechanically dissociated through $70\text{-}\mu\text{m}$ cell strainers and washed with RPMI-1640 medium containing 2% FBS. For tumor-infiltrating lymphocytes, tumor tissues were shredded into $\sim 1\text{-mm}$ -diameter pieces using scissors and digested in digestion buffer (RPMI-1640 medium containing 10% FBS, 1% penicillin/streptomycin, 10 U/ml DNase I (Roche), and $25 \mu\text{g/ml}$ Liberase TL) for 30 min at 37°C in a shaking incubator. The tissue suspension was then dissociated mechanically through a $70\text{-}\mu\text{m}$ cell filter and centrifuged at $350 \times g$ for 5 min. The supernatant was discarded, and the pellet was resuspended in 40% Percoll. The cell suspension was then gently layered on top of 80% Percoll solution. The mononuclear cell layer was collected by centrifugation at $600 \times g$ for 24 min. The cell fraction was washed before further experiments and analyses.

Flow cytometry

The obtained single-cell suspension was first treated with Fixable Viability Stain (BD Biosciences) and then incubated with an Fc receptor blocker (anti-CD16/CD32, BD Biosciences) for 10 min at room temperature. The ILC2 surface markers were stained with an antibody cocktail at 4°C for 30 min. Fluorochrome-conjugated antibodies included anti-CD3 (clone 2C11, eBioscience), anti-CD5 (clone 53-7.2, BioLegend), anti-CD45R (clone RA3-6B2, BioLegend), anti-CD11b (clone M1/70, eBioscience), anti-CD11c (clone N418, eBioscience), anti-NK1.1 (clone PK136, BioLegend), anti-Gr1 (clone RB6-8C5, BioLegend), anti-TER119 (clone TER119, BioLegend), anti-Fc ϵ R1 (clone MAR-1, eBioscience), anti-TCR γ/δ (clone UC7-13D5, BioLegend), anti-CD45.2 (clone 104, eBioscience), anti-CD90.2 (clone 53-2.1, BD Biosciences), and anti-ST2 (clone DJ8, MD BioProducts). The purity of the sorted ILC2s was confirmed using flow cytometry (96%). Mouse CD8^+ T cells were isolated from the spleen and lymph nodes using an EasySepTM Mouse CD8^+ T Cell Isolation

Kit (Stem Cell) and flow cytometry. The resulting single-cell suspension was first treated with a Fixable Viability Stain and then incubated with the Fc receptor blocker, as described above. CD8^+ T cell surface markers were stained with anti-CD3 (clone 2C11, eBioscience) and anti-CD8 (clone 53-6.7, Invitrogen) antibodies at 4°C for 30 min in the dark. The purity of the sorted CD8^+ T cells was confirmed by flow cytometry ($>99\%$). For cell proliferation detection, the antibodies used were anti-CD69 (clone H1.2F3, BioLegend). Antibodies were diluted and used according to the manufacturer's instructions. Cell sorting was performed using a FACSARIA Fusion Cell Sorter (BD Biosciences) or a FACSARIA Sorp Cell Sorter (BD Biosciences). Samples were acquired on a BD LSRFortessa, and the collected data were analyzed using FlowJo V10 (FlowJo).

ILC2 enrichment and sorting

Naïve ILC2s were obtained from mice that were intratracheally challenged with PBS. Activated ILC2s were obtained from murine airway inflammation induced by IL-33 or papain. For IL-33-induced airway inflammation, recombinant mouse IL-33 (50 ng per mouse, Biolegend) was intratracheally administered on first 4 consecutive days, and mice were sacrificed on day 7. For papain-induced airway inflammation, papain ($5 \mu\text{g}$ per mouse, Sigma-Aldrich) was intratracheally administered on 5 consecutive days, and mice were sacrificed on day 6. To obtain murine ILC2s, mouse lungs were prepared as described in Tissue Processing, and the suspension was enriched for ILC2s using EasySepTM Mouse ILC2 Enrichment Kit (STEMCELL Technologies) according to the manufacturer's protocols. Purity sort of ILC2s was identified as Lineage⁻, CD90.2^+ and ST2^+ .

FITC-dextran uptake assay

In order to test whether ILC2s have the phagocytic ability, the FITC-dextran uptake assay was performed²⁶. Activated-ILC2s sorted from IL-33-treated mice were cultured in the complete culture medium with or without FITC-dextran (Sigma). Incubate ILC2s at 4°C (used as negative control) and 37°C for 30 min protected from light. The final concentration of FITC-dextran is 0.2 mg/ml. After incubation, cells were washed three times using $1 \times \text{PBS}$ with 2% FBS to remove excess FITC-dextran. FITC-dextran-positive cells were analyzed by flow cytometry. The left gray-filled histograms represent ILC2s incubated with medium only, as negative gate setting; the open black curves represent ILC2s incubated with FITC-Dextran at 4°C ; and the open red curves represent ILC2s incubated with FITC-dextran at 37°C . The percentage of FITC-dextran positive cells in different were statistically analyzed. Data are representative of three independent replicates.

Co-culture of ILC2s with B16F10-SOVA

To test the potential ability of ILC2s to phagocytose antigen protein from tumor cells, activated ILC2s from IL-33 treatment mice lung tissue were co-cultured with B16F10-SOVA tumor

cells, which express both ovalbumin as a neo-tumor antigen and fluorescent mCherry protein to track antigen uptake by phagocytes³⁴. B16F10-SOVA cells were co-cultured with activated ILC2s at a ratio of 1:1 in RPMI 1640 medium supplemented with IL-2 (100 U/ml), IL7 (20 ng/ml), IL-33 (1 ng/ml), and 10% FBS. Half medium was replaced with fresh completed medium every other day. mCherry proteins expressed by tumor cells were tracked. The percentage of mCherry-positive ILC2s at different time points was quantified by flow cytometry. Data are representative of three independent replicates.

In vitro ILC2 culture

Freshly isolated lung ILC2s (CD45⁺Lin⁻CD90.2⁺ST2⁺) were purified from naïve or IL-33-treated C57BL/6J mice using flow cytometry. Cells (3×10^3 – 1×10^4 per well) were plated and cultured in 96-well plates in complete RPMI-1640 medium containing 10% FBS, 2 mM L-glutamine, 1% penicillin/streptomycin (Gibco), 100 U/ml IL-2 and 20 ng/ml IL-7, with or without 1 ng/ml recombinant mouse IL-33 (BioLegend), in a humidified 37°C incubator supplied with 5% carbon dioxide. When necessary, ILC2s were incubated with 1 mg/ml chicken egg OVA (Sigma) or 10 µg/ml OVA peptide 257–264. Cells were cultured for 2 or 6 days before the next experiment.

In vitro ILC2 and CD8⁺ T-cell coculture

For the proliferation assay, OT-I TCR-transgenic CD8⁺ T cells were isolated and purified as described above, and then labeled with CellTrace dye. CD8⁺ T cells were washed with PBS and stained with 1 µM CTV dye (Invitrogen) in PBS for 20 min at 37°C. The dye was removed by washing five times with culture medium containing 2% FBS. A fixed number of CTV-labeled OT-I CD8⁺ T cells (5×10^4) were mixed with IL-33 activated ILC2s (5×10^3 at an ILC2/T-cell ratio of 1:10 in 96-well plates in complete RPMI-1640 medium containing 10% FBS, 2 mM L-glutamine, 1% penicillin/streptomycin (Gibco), 100 U/ml IL-2, 20 ng/ml IL-7, and 10 ng/ml IL-15 (PeproTech). In some experiments, OVA protein (1 mg/ml) or OVA peptide 257–264 (10 µg/ml) was added to the coculture system. For cytokine detection, supernatants from co-cultures of antigen-stimulated ILC2-CD8⁺ T cells were harvested after 72 h of culture. The levels of cytokines in the culture supernatants were measured by ELISA (mouse IFN-gamma DuoSet ELISA kit, R&D system, DY485, mouse TNF-alpha DuoSet ELISA kit, R&D system, DY410). And the GZMB production was detected by flow cytometry after 72 h of culture (clone NGZB, Invitrogen).

LDH cytotoxicity detection

The LDH Cytotoxicity Assay Kit was purchased from Beyotime (C0016, Beyotime). Experiments were performed according to the manufacturer's protocol. Briefly, 1×10^4 B16F10-OVA tumor cells were seeded in 48-well plates 1 day prior to establishing the co-culture system. A total of 1×10^5 OT-I CD8⁺ T cells mixed with ILC2s or ILC2s previously loaded with OVA were added to adherent tumor cells. Simultaneously, OT-I CD8⁺ T cells alone, ILC2s

alone, or previously OVA-loaded ILC2s alone were added to the tumor cell culture system as controls. After 48 h, the culture supernatant was aspirated from each well. The reagents in the kit were successively added to the test samples as described in the protocols. The absorbance of all test samples was measured using a 450-nm filter. The results were used to calculate LDH release from tumor cells using a standard curve. The relative value was calculated based the formula: (Absorbance of sample – Absorbance of control sample)/(Absorbance of the maximum enzyme activity of the cell-Absorbance of control sample) × 100%.

RNA-seq and data analysis

Approximately 5000–20000 ILC2s from different mouse models were sorted using TRIzol™ Reagent (Invitrogen) lysis buffer. Total RNA was prepared and processed to generate a cDNA library using the TruePrep™ DNA Library Prep Kit V2 for Illumina® (Vazyme, TD503–01), according to the manufacturer's protocol. RNA-seq libraries were sequenced on the Illumina HiSeq PE150 platform. Differential gene expression was defined as a twofold change and *p* value < 0.05. GSEA was performed using the GSEA software. A public dataset (GEO: GSE184976) was used to investigate the expression of MHC class I-associated and costimulatory molecules in WT DCs after LPS stimulation. FPKM values were visualized using the R package pheatmap (1.0.12).

Statistical analysis

Prism v.8 and v.9 (GraphPad Software) were used for statistical analysis. Data are represented as mean ± SEM or SD. For two-group comparisons, two-tailed unpaired Student's t-test was used. For multiple group comparisons, one-way ANOVA was performed. For time-course comparisons, two-way analysis of variance (ANOVA) was used. Differences were considered significant at **p* < 0.05, ** *p* < 0.01, *** *p* < 0.001, and **** *p* < 0.0001; NS indicates not significant.

Disclosure statement

No potential conflict of interest was reported by the authors.

Funding

This work was supported by the National Key Research and Development Program of China (2018YFA0507402), the National Natural Science Foundation of China (32000667), the Shanghai Science and Technology Innovation Action (21ZR1470600, 21JC1405800 and 20S11901800), Shanghai Hospital Development Center (SHDC22021217), and the Youth Innovation Promotion Association of the Chinese Academy of Sciences (2022264).

Author contributions

Wen and Zhang designed the experiments and prepared the figures. J. Wen, R. Wang, Y. Zhang, S. Cheng, Y. Huang, and L. Xu performed experiments. J. Wen, Y. Zhang, and S. Cheng analyzed the data. L. Ma and

Z. Ling provided material support. Wen, Sun, and Zhang interpreted the results and wrote the manuscript. B. Sun, Y. Zhang, D. Zhao and J. Xu supervised the project.

Data availability statement

The data that support the findings of this study are available from the corresponding author, B. Sun, upon reasonable request.

References

- Gurram RK, Zhu J. Orchestration between ILC2s and Th2 cells in shaping type 2 immune responses. *Cell Mol Immunol.* 2019;16(3):225–235. doi:10.1038/s41423-019-0210-8.
- Mjösberg J, Bernink J, Golebski K, Karrich J, Peters C, Blom B, Te Velde A, Fokkens W, van Druenen C, Spits H, et al. The transcription factor GATA3 is essential for the function of human type 2 innate lymphoid cells. *Immunity.* 2012;37(4):649–659. doi: 10.1016/j.immuni.2012.08.015.
- Ferreira ACF, Szeto ACH, Heycock MWD, Clark PA, Walker JA, Crisp A, Barlow JL, Kitching S, Lim A, Gogoi M, et al. ROR α is a critical checkpoint for T cell and ILC2 commitment in the embryonic thymus. *Nat Immunol.* 2021;22(2):166–178. doi: 10.1038/s41590-020-00833-w.
- Eberl G, Colonna M, Di Santo JP, McKenzie AN. Innate lymphoid cells. Innate lymphoid cells: a new paradigm in immunology. *Sci.* 2015;348(6237):aaa6566. doi:10.1126/science.aaa6566.
- Oliphant CJ, Hwang Y, Walker J, Salimi M, Wong S, Brewer J, Englezakis A, Barlow J, Hams E, Scanlon S, et al. MHCII-mediated dialog between group 2 innate lymphoid cells and CD4(+) T cells potentiates type 2 immunity and promotes parasitic helminth expulsion. *Immunity.* 2014;41(2):283–295. doi: 10.1016/j.immuni.2014.06.016.
- Ercolano G, Falquet M, Vanoni G, Trabanelli S, Jandus C. ILC2s: New actors in tumor immunity. *Front Immunol.* 2019;10:2801. doi:10.3389/fimmu.2019.02801.
- Spits H, Mjösberg J. Heterogeneity of type 2 innate lymphoid cells. *Nat Rev Immunol.* 2022;22(11):1–12. doi:10.1038/s41577-022-00704-5.
- Trabanelli S, Curti A, Lecciso M, Salome B, Riether C, Ochsenbein A, Romero P, Jandus C. CD127+ innate lymphoid cells are dysregulated in treatment naïve acute myeloid leukemia patients at diagnosis. *Haematologica.* 2015;100(7):e257–260. doi:10.3324/haematol.2014.119602.
- Chevalier MF, Trabanelli S, Racle J, Salomé B, Cesson V, Gharbi D, Bohner P, Domingos-Pereira S, Dartiguenave F, Fritschi A-S, et al. ILC2-modulated T cell-to-MDSC balance is associated with bladder cancer recurrence. *J Clin Invest.* 2017;127(8):2916–2929. doi: 10.1172/JCI89717.
- Trabanelli S, Chevalier MF, Martinez-Usatorre A, Gomez-Cadena A, Salomé B, Lecciso M, Salvestrini V, Verdeil G, Racle J, Papayannidis C, et al. Tumour-derived PGD2 and NKp30-B7H6 engagement drives an immunosuppressive ILC2-MDSC axis. *Nat Commun.* 2017;8(1):593. doi: 10.1038/s41467-017-00678-2.
- Jacquetot N, Seillet C, Wang M, Pizzolla A, Liao Y, Hediye-Zadeh S, Grisaru-Tal S, Louis C, Huang Q, Schreuder J, et al. Blockade of the co-inhibitory molecule PD-1 unleashes ILC2-dependent anti-tumor immunity in melanoma. *Nat Immunol.* 2021;22(7):851–864. doi: 10.1038/s41590-021-00943-z.
- Moral JA, Leung J, Rojas LA, Ruan J, Zhao J, Sethna Z, Ramnarain A, Gasmi B, Gururajan M, Redmond D, et al. ILC2s amplify PD-1 blockade by activating tissue-specific cancer immunity. *Nature.* 2020;579(7797):130–135. doi: 10.1038/s41586-020-2015-4.
- Howard E, Hurrell BP, Helou DG, Quach C, Painter JD, Shafiei-Jahani P, Fung M, Gill PS, Soroosh P, Sharpe AH, et al. PD-1 blockade on tumor microenvironment-resident ILC2s promotes TNF- α production and restricts progression of metastatic melanoma. *Front Immunol.* 2021;12:733136. doi:10.3389/fimmu.2021.733136.
- Wan J, Wu Y, Huang L, Tian Y, Ji X, Abdelaziz MH, Cai W, Dineshkumar K, Lei Y, Yao S, et al. ILC2-derived IL-9 inhibits colorectal cancer progression by activating CD8(+) T cells. *Cancer Lett.* 2021;502:34–43. doi:10.1016/j.canlet.2021.01.002.
- Sonnenberg GF, Hepworth MR. Functional interactions between innate lymphoid cells and adaptive immunity. *Nat Rev Immunol.* 2019;19(10):599–613. doi:10.1038/s41577-019-0194-8.
- Pelly VS, Kannan Y, Coomes SM, Entwistle LJ, Rückerl D, Seddon B, MacDonald AS, McKenzie A, Wilson MS. IL-4-producing ILC2s are required for the differentiation of T(H)2 cells following Heligmosomoides polygyrus infection. *Mucosal Immunol.* 2016;9(6):1407–1417. doi:10.1038/mi.2016.4.
- Noval Rivas M, Burton OT, Oettgen HC, Chatila T. IL-4 production by group 2 innate lymphoid cells promotes food allergy by blocking regulatory T-cell function. *J Allergy Clin Immunol.* 2016;138(3):801–811.e809. doi:10.1016/j.jaci.2016.02.030.
- Moro K, Yamada T, Tanabe M, Takeuchi T, Ikawa T, Kawamoto H, Furusawa J-I, Ohtani M, Fujii H, Koyasu S, et al. Innate production of T(H)2 cytokines by adipose tissue-associated c-Kit(+)/Sca-1(+) lymphoid cells. *Nature.* 2010;463(7280):540–544. doi: 10.1038/nature08636.
- Jackson-Jones LH, Duncan SM, Magalhaes MS, Campbell SM, Maizels RM, McSorley HJ, Allen JE, Bénézech C. Fat-associated lymphoid clusters control local IgM secretion during pleural infection and lung inflammation. *Nat Commun.* 2016;7(1):12651. doi:10.1038/ncomms12651.
- Molofsky AB, Van Gool F, Liang H-E, Van Dyken S, Nussbaum J, Lee J, Bluestone J, Locksley R. Interleukin-33 and interferon- γ counter-regulate group 2 innate lymphoid cell activation during immune perturbation. *Immunity.* 2015;43(1):161–174. doi:10.1016/j.immuni.2015.05.019.
- Webb GJ, Hirschfield GM, Lane PJ. OX40, OX40L and autoimmunity: a comprehensive review. *Clin Rev Allergy Immunol.* 2016;50(3):312–332. doi:10.1007/s12016-015-8498-3.
- Hardman CS, Chen Y-L, Salimi M, Jarrett R, Johnson D, Järvinen VJ, Owens RJ, Repapi E, Cousins DJ, Barlow JL, et al. Ccl1a presentation of endogenous antigens by group 2 innate lymphoid cells. *Sci Immunol.* 2017;2(18). doi:10.1126/sciimmunol.aan5918.
- Boon T, Cerottini JC, Van den Eynde B, van der Bruggen P, Van Pel A. Tumor antigens recognized by T lymphocytes. *Annu Rev Immunol.* 1994;12(1):337–365. doi:10.1146/annurev.iy.12.040194.002005.
- Anderson CK, Brossay L. The role of MHC class Ib-restricted T cells during infection. *Immunogenetics.* 2016;68(8):677–691. doi:10.1007/s00251-016-0932-z.
- Chen L, Flies DB. Molecular mechanisms of T cell co-stimulation and co-inhibition. *Nat Rev Immunol.* 2013;13(4):227–242. doi:10.1038/nri3405.
- Bürdek M, Spranger S, Wilde S, Frankenberger B, Schendel DJ, Geiger C. Three-day dendritic cells for vaccine development: antigen uptake, processing and presentation. *J Transl Med.* 2010;8(1):90. doi:10.1186/1479-5876-8-90.
- Liu L, Ye TH, Han YP, Song H, Zhang YK, Xia Y, Wang NY, Xiong Y, Song XJ, Zhu YX, et al. Reductions in myeloid-derived suppressor cells and lung metastases using AZD4547 treatment of a metastatic murine breast tumor model. *Cell Physiol Biochem.* 2014;33(3):633–645. doi: 10.1159/000358640.
- Okuyama Y, Okajima A, Sakamoto N, Hashimoto A, Tanabe R, Kawajiri A, Kawabe T, Ishii N. IL-33-ILC2 axis promotes anti-tumor CD8(+) T cell responses via OX40 signaling. *Biochem Biophys Res Commun.* 2022;637:9–16. doi:10.1016/j.bbrc.2022.11.006.
- Huang MN, Nicholson LT, Batich KA, Swartz AM, Kopin D, Wellford S, Prabhakar VK, Woroniecka K, Nair SK, Fecci PE, et al. Antigen-loaded monocyte administration induces potent

- therapeutic antitumor T cell responses. *J Clin Invest.* 2020;130(2):774–788. doi: [10.1172/JCI128267](https://doi.org/10.1172/JCI128267).
30. Filley AC, Dey M. Dendritic cell based vaccination strategy: an evolving paradigm. *J Neurooncol.* 2017;133(2):223–235. doi: [10.1007/s11060-017-2446-4](https://doi.org/10.1007/s11060-017-2446-4).
31. Lehmann FM, von Burg N, Ivanek R, Teufel C, Horvath E, Peter A, Turchinovich G, Staehli D, Eichlisberger T, Gomez de Agüero M, et al. Microbiota-induced tissue signals regulate ILC3-mediated antigen presentation. *Nat Commun.* 2020;11(1):1794. doi: [10.1038/s41467-020-15612-2](https://doi.org/10.1038/s41467-020-15612-2).
32. Grigg JB, Shanmugavadivu A, Regen T, Parkhurst CN, Ahmed A, Joseph AM, Mazzucco M, Gronke K, Diefenbach A, Eberl G, et al. Antigen-presenting innate lymphoid cells orchestrate neuroinflammation. *Nature.* 2021;600(7890):707–712. doi: [10.1038/s41586-021-04136-4](https://doi.org/10.1038/s41586-021-04136-4).
33. Roberts EW, Broz ML, Binnewies M, Headley MB, Nelson AE, Wolf DM, Kaisho T, Bogunovic D, Bhardwaj N, Krummel MF, et al. Critical role for CD103(+)/CD141(+) dendritic cells bearing CCR7 for tumor antigen trafficking and priming of T cell immunity in melanoma. *Cancer Cell.* 2016;30(2):324–336. doi: [10.1016/j.ccell.2016.06.003](https://doi.org/10.1016/j.ccell.2016.06.003).
34. Nouri-Shirazi M, Banchereau J, Bell D, Burkeholder S, Kraus ET, Davoust J, Palucka KA. Dendritic cells capture killed tumor cells and present their antigens to elicit tumor-specific immune responses. *J Immunol (Baltimore, Md. : 1950).* 2000;165(7):3797–3803. doi: [10.4049/jimmunol.165.7.3797](https://doi.org/10.4049/jimmunol.165.7.3797).